A NON-HOMOGENEOUS MRF MODEL FOR MULTIRESOLUTION BAYESIAN ESTIMATION

Suhail S. Saquib and Charles A. Bouman

School of Electrical Engineering
Purdue University
West Lafayette, IN 47907.

Ken Sauer

Department of Electrical Engineering
University of Notre Dame
Notre Dame, IN 46556.

ABSTRACT

The popularity of Bayesian methods in image processing applications has generated great interest in image modeling. A good image model needs to be non-homogeneous to be able to adapt to the local characteristics of the different regions in an image. In the past however, such a formulation was difficult since it was not clear as to how to choose the parameters of the non-homogeneous model. But now motivated by recent results in ML parameter estimation of MRF models, we formulate in this paper a non-homogeneous MRF image model in the multiresolution framework. The advantage of the multiresolution framework is two fold: First, it makes it possible to estimate the parameters of the non-homogeneous MRF at any resolution by using the image at the coarser resolution. Second, it yields multiresolution algorithms which are computationally efficient and more robust than their single resolution counterparts. Experimental results in tomographic image reconstruction and optical flow computation problems verify the superior modeling provided by the new model.

1. INTRODUCTION

In the past decade, Bayesian methods have gained popularity in image processing applications such as computerized tomography [1], image restoration [2] and the computation of optical flow [3] to name a few. Consequently image modeling has become increasingly important. Since natural images often have regions with different local characteristics, it is imperative for a good image model to be non-homogeneous to adapt to the local behavior of the image. Past approaches to solve this modeling problem have resulted in Markov random field (MRF) models with line processes [2] and doubly stochastic MRFs [4]. However explicitly using line elements adds to the complexity of the problem considerably by increasing the dimensionality of the required optimization. In addition, optimal parameter estimation of these models is also difficult.

On the other hand, homogeneous MRF image models have been widely used because of their relatively simple parametrization. These models are usually specified in terms of a potential function that assigns cost to the differences between neighboring pixels. The form of this potential function is crucial to the preservation of edges in the estimated image. A host of edge-preserving potential functions have been proposed in the literature [5]. In particular, we will be using the generalized Gaussian MRF (GGMRF) as the basis of our new model since it has been shown to yield good edge-preservation [6]. Recent results on the ML parameter estimation of the GGMRF model [7] has motivated us to formulate a non-homogeneous GGMRF model in the multiresolution framework. The key to the formulation of the new model lies in two important factors: First, the form of the ML estimate of the scale parameter of the homogeneous GGMRF model gives us a clue to choose the scale parameters adaptively in the new model. Second, the multiresolution framework allows us to estimate these scale parameters at each pixel by using the image at the previous coarser resolution.

The new image model automatically gives rise to multiresolution algorithms that estimate the image at progressively finer resolutions. This is very desirable since multiresolution algorithms have generated a lot of interest in image processing applications due to their faster convergence and better image modeling [8, 9]. Multiresolution methods are also particularly well suited to problems such as the optical flow computation, since they can more effectively avoid being trapped in some local minima than their single resolution counterparts. In this paper, we apply our new model to the optical flow computation and the tomographic reconstruction problems to evaluate the effectiveness of the model. Experimental results suggest that the new non-homogeneous GGMRF model yields improved performance over the corresponding homogeneous GGMRF model.

2. NEW IMAGE MODEL

We will denote the image at scale k by the random field $X^{(k)}$ and the set of lattice points by $S^{(k)}$. Let L be the coarsest resolution. Then at resolution L we define $X^{(L)}$ to be a homogeneous GGMRF [6] given as

$$\log P(x^{(L)}|T_L) = \frac{-1}{T_L} \sum_{\{i,j\}\in\mathcal{N}} b_{i-j} \left| x_i^{(L)} - x_j^{(L)} \right|^p$$

THIS WORK WAS SUPPORTED BY NATIONAL SCIENCE FOUNDATION GRANT NUMBER MIP93-00560.

APPEARED IN THE *IEEE INT'L CONF. ON IMAGE PROC.*, VOL. 2, PP. 445-448, LAUSANNE SWITZERLAND, SEPT. 16-19, 1996.

where T_L is the temperature parameter at resolution L and $\mathcal{N}$ denotes the neighborhood. For all finer resolutions, $k = 0, \ldots, L-1$, we define $X^{(k)}$ to be a non-homogeneous GGMRF given as

$$\log P(x^{(k)}|x^{(k+1)}, T_k) = \frac{-1}{T_k} \sum_{\{i,j\}\in\mathcal{N}} \frac{b_{i-j}}{p\sigma_{ij}^p(x^{(k+1)})} \left|x_i^{(k)} - x_j^{(k)}\right|^p \qquad (1)$$

where $\sigma_{ij}(x^{(k+1)})$ is the scale parameter estimated from the coarser resolution image $x^{(k+1)}$ for the link between pixels i and j and T_k is the overall temperature parameter. Note that the MRF now is non-homogeneous since the scale parameter, $\sigma_{ij}(\cdot)$, is varying spatially. Let

$$Ix^{(k)} = I_{k+1}^k x^{(k+1)}$$

where I_{k+1}^k is the interpolating matrix from scale $k+1$ to k. Then motivated by the form of the ML estimate of the scale parameter for a GGMRF [7] we define $\sigma_{ij}(x^{(k+1)})$ as follows

$$\sigma_{ij}^p(x^{(k+1)}) = \frac{\sigma_i^p(x^{(k+1)}) + \sigma_j^p(x^{(k+1)})}{2}$$

where $\forall i \in S^{(k)}$

$$\sigma_i^p(x^{(k+1)}) = \sum_{j\in\mathcal{N}_i} b_{i-j} \left|Ix_i^{(k)} - Ix_j^{(k)}\right|^p$$

Here $\sigma_i(\cdot)$ is the scale parameter estimated at pixel i by using only neighboring pixels. The scale parameter for the link between i and j is then just the average of the corresponding scale parameters for pixels i and j.

3. DATA MODEL

Let y be the measured data. In the tomography problem, y denotes the photon counts recorded at the detectors and is Poisson distributed. In the optical flow problem, $y(t)$ is the intensity image recorded by the camera at time instance t.

3.1. Tomography

Let $A^{(0)}$ be the projection matrix of the tomographic system and $A_{i*}^{(0)}$ denote the i^{th} row of $A^{(0)}$. Then the log likelihood at scale 0 has a similar form for emission and transmission tomography and is given as

$$\log P(y|x^{(0)}) = -\sum_{i=1}^{M} f_i(A_{i*}^{(0)} x^{(0)})$$

where M is the number of projections and $f_i(\cdot)$ are convex functions. For scales $k > 0$, the form of the log likelihood is given as [9]

$$\log P(y|x^{(k)}) = -\sum_{i=1}^{M} f_i(A_{i*}^{(0)} I_k^0 x^{(k)}) = -\sum_{i=1}^{M} f_i(A_{i*}^{(k)} x^{(k)})$$

where $A^{(k)} = A^{(0)} I_k^0$.

3.2. Optical Flow

In this case, x denotes the field of vector displacements that represents the optical flow. Let $t = 0, 1, 2$ be three time instances at which we have the intensity image $y(t)$. Let the interpolated displacement field at scale 0 from any scale k be denoted as

$$Ix^{(0)} = I_k^0 x^{(k)}$$

Then the particular form of the log likelihood we use is given by

$$\log P(y|x^{(k)}) = \max\left\{\log P_f(y|x^{(k)}), \log P_b(y|x^{(k)})\right\}$$

where

$$\begin{aligned}
\log P_f(y|x^{(k)}) &= -\frac{1}{2\sigma^2} \sum_{s\in S^{(0)}} \left(y_s(1) - y_{s+Ix_s^{(0)}}(2)\right)^2 \\
\log P_b(y|x^{(k)}) &= -\frac{1}{2\sigma^2} \sum_{s\in S^{(0)}} \left(y_s(1) - y_{s-Ix_s^{(0)}}(0)\right)^2
\end{aligned}$$

Note that by using the forward and backward prediction of the displacement field we can explicitly account for occluded and revealed points in the image sequence. The data model assumes that the intensity image is corrupted with additive Gaussian noise of variance σ^2.

4. PARAMETER ESTIMATION

The ML estimate of T_k for the proposed model can be obtained easily at each resolution by using the result of [7]

$$\hat{T}_L(x^{(L)}) = \frac{p}{N_L} \sum_{\{i,j\}\in\mathcal{N}} b_{i-j} \left|x_i^{(L)} - x_j^{(L)}\right|^p$$

$$\hat{T}_k(x^{(k)}, x^{(k+1)}) = \frac{p}{N_k} \sum_{\{i,j\}\in\mathcal{N}} \frac{b_{i-j}}{p\sigma_{ij}^p(x^{(k+1)})} \left|x_i^{(k)} - x_j^{(k)}\right|^p$$

for $k \neq L$. Here N_k is the number of pixels at resolution k. However, for an unsupervised scheme, we need to estimate T_k directly from the data y. The EM algorithm is employed in this case to address the incomplete data problem and compute the estimates. This results in an iterative procedure where the parameter is updated with each iteration t in the following fashion

$$\hat{T_L}^{t+1} = E\left[\hat{T}_L(X^{(L)})|Y = y, \hat{T_L}^t\right]$$

$$\hat{T_k}^{t+1} = E\left[\hat{T}_k(X^{(k)}, x^{(k+1)})|Y = y, X^{(k+1)} = x^{(k+1)}, \hat{T_k}^t\right]$$

for $k \neq L$. The involved expectation required in the EM update is numerically computed by using the fast stochastic simulation technique proposed in [7].

5. EXPERIMENTAL RESULTS

In order to evaluate the performance of the proposed model we apply it to the tomographic image reconstruction and the optical flow computation problem. The sequential MAP

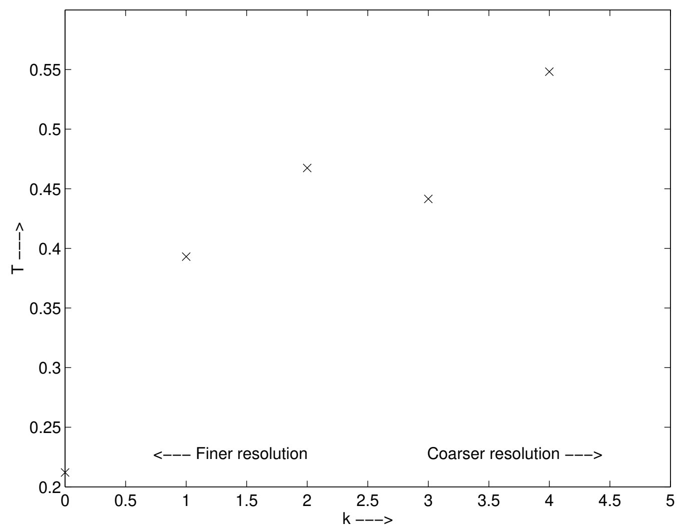

Figure 1: Estimated temperature T_k for $k = 0, \ldots, 4$ for the PET data using the EM algorithm.

(SMAP) [9] estimator is used to compute the reconstructions. At each resolution, the iterative coordinate descent algorithm is used for solving the optimization problem.

The 3-D PET data that we use for the tomography problem was obtained from cardiac perfusion imaging using Tc-99m sestamibi. For each slice, 128 projections were taken at 120 uniformly spaced angles between 0 and 2π. Fig. 2 shows the convolution back projected (CBP) image of one of the slices for a male patient. The total photon count for this slice was 148761.

Fig. 1 shows the temperature T_k that was estimated at each resolution using the EM algorithm for the PET data. Fig. 2 shows the reconstruction using a single resolution homogeneous GGMRF ($p = 1.1$) and the reconstruction at the finest resolution using the non-homogeneous GGMRF ($p = 1.1$). For the homogeneous GGMRF the temperature parameter was manually chosen to yield the most visually appealing result. On the other hand, the temperature parameter for the non-homogeneous GGMRF was automatically estimated at each resolution. Note that the multiresolution image appears to be clean and sharp. However, further testing needs to be done in cases where ground truth is known to validate the performance of the non-homogeneous GGMRF model.

Fig. 3 shows the first and the third frames of the synthetic image sequence used to compute the optical flow. Two dimensional separable sine waves with additive white Gaussian noise were used to generate the images. The object is moving one pixel per frame diagonally upwards to the left and the background is moving 1.5 pixels per frame diagonally downwards to the right. The variance of the additive Gaussian noise is assumed to be unknown and is directly estimated from the data along with the scale parameters for the image model.

Fig. 3 shows the true optical flow in comparison to the flow obtained using a homogeneous GGMRF ($p = 1.0$) and the proposed non-homogeneous GGMRF ($p = 1.0$). Note that in both cases the estimation was done in the multiresolution framework. The coarse resolution optical flow was used to initialize the flow at the next finer resolution. A single scale parameter was used for the homogeneous case while the scale parameter was space varying in the non-homogeneous case. Clearly the non-homogeneous field model preserves the discontinuity in the flow field much better than the homogeneous field model.

Acknowledgement

The authors would like to thank Tin-Su Pan & Michael A. King of the University of Massachusetts for providing the PET data.

6. REFERENCES

[1] E. Levitan and G. Herman, "A maximum a *posteriori* probability expectation maximization algorithm for image reconstruction in emission tomography," *IEEE Trans. on Medical Imaging*, vol. MI-6, pp. 185–192, Sept. 1987.

[2] S. Geman and D. Geman, "Stochastic relaxation, Gibbs distributions and the Bayesian restoration of images," *IEEE Trans. on Pattern Analysis and Machine Intelligence*, vol. PAMI-6, pp. 721–741, Nov. 1984.

[3] J. Konrad and E. Dubois, "Bayesian estimation of motion vector fields," *IEEE Trans. on Pattern Analysis and Machine Intelligence*, vol. 14, no. 9, pp. 910–927, September 1992.

[4] J. Woods, S. Dravida, and R. Mediavilla, "Image estimation using double stochastic Gaussian random field models," *IEEE Trans. on Pattern Analysis and Machine Intelligence*, vol. PAMI-9, no. 2, pp. 245–253, March 1987.

[5] K. Lange, "Convergence of EM image reconstruction algorithms with Gibbs smoothing," *IEEE Trans. on Medical Imaging*, vol. 9, no. 4, pp. 439–446, December 1990.

[6] C. A. Bouman and K. Sauer, "A generalized Gaussian image model for edge-preserving map estimation," *IEEE Trans. on Image Processing*, vol. 2, pp. 296–310, July 1993.

[7] S. S. Saquib, C. A. Bouman, and K. Sauer, "ML parameter estimation for Markov random fields, with applications to Bayesian tomography," Tech. Rep. TR-ECE 95-24, School of Electrical and Computer Engineering, Purdue University, West Lafayette, IN 47907, October 1995.

[8] M. R. Luettgen, W. C. Karl, and A. S. Willsky, "Efficient multiscale regularization with applications to the computation of optical flow," *IEEE Trans. on Image Processing*, vol. 3, no. 1, January 1994.

[9] S. S. Saquib, C. A. Bouman, and K. Sauer, "A new multiscale image model for Bayesian tomography," *Proc. of the Image and Multidimensional Signal Proc. Workshop*, March 3-6 1996, Belize City, Belize.

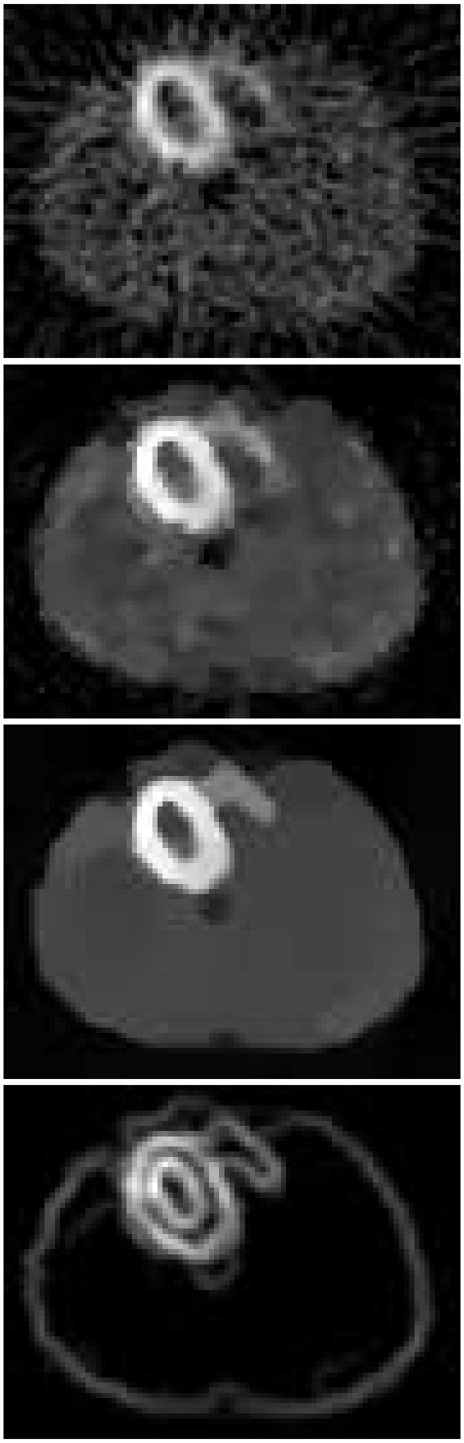

Figure 2: From top to bottom a) CBP image, b) Reconstruction using a single resolution homogeneous GGMRF prior with $p = 1.1$ with scale parameter chosen for best visual appearance, c) Reconstruction at finest resolution using the multiresolution non-homogeneous GGMRF model with $p = 1.1$, d) Scale parameters $\sigma_i(\cdot)$ for each pixel at the finest resolution. (Phantom courtesy of Tin-Su Pan & Michael A. King, Univ. of Massachusetts.)

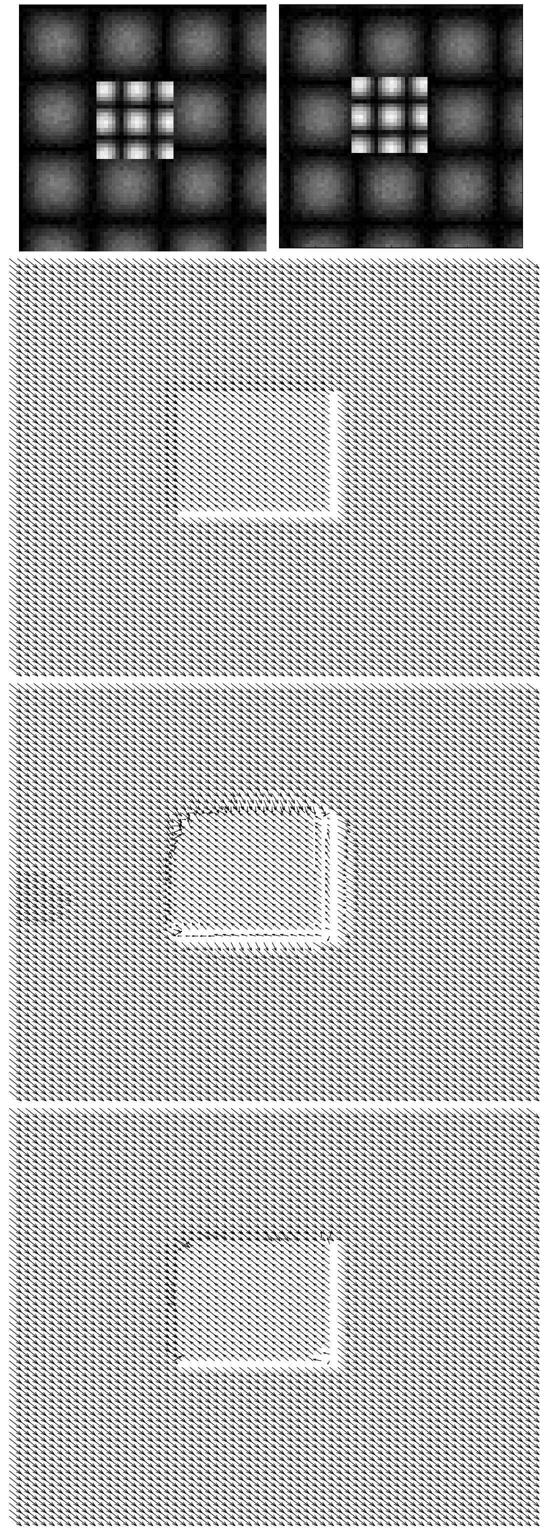

Figure 3: From top to bottom a) Two frames of the image sequence, b) True optical flow, Estimated flow using the c) homogeneous GGMRF with $p = 1.0$, and d) non-homogeneous GGMRF with $p = 1.0$.